Brief Report

DOI: 10.5582/bst.2026.01046

Biallelic inactivation of *EXT1* in patient-derived iPSCs confirms the "Two-hit" hypothesis in hereditary multiple osteochondromas

Yali Yang[1,2,3], Zhenzhong Han[1,2,3], Guowei Li[1,2,3], Zihan Li[1,2,3], Chonghao Shao[1,2,3], Wentao Li[1,2,3], Jing Wang[1,2,3], Jing Luan[1,2,3,*], Yazhou Cui[1,2,3,4,*], Jinxiang Han[1,2,3,*]

[1] Biomedical Sciences College, Shandong Medicinal Biotechnology Centre, Shandong First Medical University & Shandong Academy of Medical Sciences, Ji'nan, Shandong, China;
[2] Department of Orthopedic Surgery, The First Affiliated Hospital of Shandong First Medical University, Ji'nan, Shandong, China;
[3] Key Lab for Biotech-Drugs of National Health Commission, Ji'nan, Shandong, China;
[4] Qingdao Academy of Chinese Medical Science, Shandong University of Traditional Chinese Medicine, Ji'nan, Shandong, China.

SUMMARY: Hereditary Multiple Osteochondromas (HMO) is a rare autosomal dominant skeletal disorder caused by heterozygous loss-of-function mutations in *EXT1* or *EXT2*, which encode glycosyltransferases essential for heparan sulfate (HS) biosynthesis. Whether haploinsufficiency alone suffices or biallelic inactivation is required for osteochondroma formation remains a central unresolved question. In this study, we employed CRISPR/Cas9 combined with PiggyBac transposon technology to introduce a second pathogenic mutation (c.1883+1G>T) into patient-derived induced pluripotent stem cells (iPSCs) carrying a heterozygous EXT1 c.1126C>T mutation. This approach enabled the generation of isogenic iPSC lines: wild-type (WT), single-mutant (SM), and double-mutant (DM). These iPSCs were differentiated through induced mesenchymal stem cells (iMSCs) into chondrocytes. Biallelic *EXT1* mutation in DM cells led to significant upregulation of *SOX9*, *COL2A1*, and *ACAN*, elevated glycosaminoglycan (GAG) levels, and markedly reduced HS, whereas SM cells remained indistinguishable from WT. Three-dimensional (3D) chondrogenic organoid cultures revealed that DM organoids were enlarged and structurally disorganized, partially recapitulating key histopathological features of osteochondromas. Transcriptomic analysis identified the Wnt signaling pathway as the most significantly enriched pathway among differentially expressed genes following *EXT1* loss. Collectively, these findings provide direct human cellular evidence that complete EXT1 inactivation—not haploinsufficiency—drives aberrant chondrogenesis, likely through impaired sequestration of morphogen ligands, thereby supporting the Two-hit pathogenic model.

Keywords: hereditary multiple osteochondromas, heparan sulfate, chondrogenesis, Two-hit hypothesis, Wnt signaling pathway, ligand sequestration

1. Introduction

Hereditary Multiple Osteochondromas (HMO) is a rare autosomal dominant skeletal disorder caused by loss-of-function mutations in *exostosin glycosyltransferase 1* (*EXT1*) or *exostosin glycosyltransferase 2* (*EXT2*) (*1*). *EXT1* mutations account for 60–70% of all HMO cases, and the global prevalence of HMO is approximately 1/50000 (*2*). Up to 5% of affected patients undergo malignant transformation to secondary peripheral chondrosarcoma (*3*). EXT1 and EXT2 assemble into a heteromeric complex within the endoplasmic reticulum (ER) before translocating to the Golgi apparatus, where the complex catalyzes heparan sulfate (HS) chain polymerization through the alternating addition of N-acetylglucosamine (GlcNAc) and glucuronic acid residues (GlcA) (*4*) (Figure 4A). As a critical component of heparan sulfate proteoglycans (HSPGs), HS fine-tunes the spatial distribution and signaling activity of multiple morphogens—including Indian Hedgehog (IHH), fibroblast growth factors (FGFs), bone morphogenetic proteins (BMPs), and Wnt family ligands—thereby maintaining chondrocyte proliferation, differentiation, and columnar organization within the growth plate (*5,6*). Studies in *Ext1*-deficient mice have demonstrated aberrant IHH signaling gradients and consequent skeletal patterning defects (*7*), and zebrafish *dackel* (*ext2*) mutants display severe chondrocyte stacking disorganization (*8*).

Knudson originally proposed the Two-hit hypothesis in the context of retinoblastoma, positing that tumor suppressor gene inactivation requires loss of both

functional alleles (*9*). This model has since been extended to HMO, where accumulating evidence suggests that osteochondroma formation requires biallelic *EXT* inactivation through loss of heterozygosity (LOH) at the somatic level (*10,11*). Heterozygous *Ext* mice develop no osteochondromas, whereas conditional biallelic knockout in chondrocytes or perichondrial progenitor cells recapitulates the full spectrum of HMO skeletal pathology (*10,11*). De Andrea *et al.* demonstrated that heterozygous *EXT* mutations do not compromise chondrogenic differentiation capacity in human bone marrow-derived mesenchymal stem cells, and further detected LOH in 63% of surgically resected osteochondromas (*12*). Nevertheless, inherent species differences between murine models and human disease, together with the limited availability of patient-derived osteochondroma specimens for molecular analysis, have constrained the ability to establish direct genotype–phenotype relationships in a controlled human cellular context.

To address these limitations, we employed patient-derived induced pluripotent stem cells (iPSCs) combined with footprint-free CRISPR/Cas9–PiggyBac genome editing to reconstitute the Two-hit event *in vitro* within a fully isogenic human system. HSPGs are known to regulate Wnt ligand distribution and signal transduction *(13)*. We therefore examined how graded EXT1 loss, from monoallelic to biallelic, affects Wnt pathway activity, aiming to provide mechanistic support for the Two-hit model.

2. Materials and Methods

2.1. sgRNA design and HDR donor construction

sgRNAs targeting the splice donor site of *EXT1* intron 9 (c.1883+1G) were designed using CRISPOR (*http://crispor.tefor.net*) and cloned into lentiCRISPRv2 (Addgene, USA; #52961). An HDR donor was constructed with ~650 bp homology arms flanking a PiggyBac ITR-bracketed PuroΔTK dual-selection cassette, with the left arm harboring the desired c.1883+1G>T mutation.

2.2. iPSCs culture and genome editing

Patient-derived iPSCs (male; heterozygous *EXT1 c.1126C>T*; informed consent under ethics approval) were maintained on Matrigel® (Corning, Corning, NY, USA)-coated plates in mTeSR™ Plus (STEMCELL Technologies, Vancouver, BC, Canada) at 37°C/5% CO_2. At ~80% confluency, iPSCs were co-transfected with Cas9–sgRNA and HDR donor using Lipofectamine™ 3000 (Thermo Fisher Scientific, USA) with 10 μM Y-27632. After 14-day puromycin selection, the PiggyBac cassette was excised *via* hyPBase transposase and acyclovir negative selection. Site-specific integration was verified by junction PCR (P1/P2). Following PiggyBac excision, PCR using primers P3/P4 designed within the transposon cassette sequence confirmed complete cassette removal by the absence of amplification products. Footprint-free excision was further confirmed by Sanger sequencing. The biallelic mutant (c.1126C>T + c.1883+1G>T) was designated double-mutant (DM); parental heterozygous iPSCs as single-mutant (SM); and an isogenic wild-type clone as WT control.

2.3. iMSC induction and chondrogenic differentiation

iPSCs were differentiated into iMSCs using the StemMACS™ MSC Differentiation Kit (STEMCELL Technologies). For 2D chondrogenesis, iMSCs (passage 4–6) were cultured on gelatin-coated plates in high-glucose DMEM (Gibco, USA) with 10 ng/mL TGF-β1 (PeproTech, USA), 100 nM dexamethasone, 50 μg/mL ascorbate-2-phosphate (Sigma-Aldrich), 1% ITS, and 1% penicillin–streptomycin (Gibco) for 21 days. For 3D culture, 2.5×10^5 iMSCs were pelleted (300 × g, 5 min) in 15 mL conical tubes and maintained in suspension culture with identical medium for 21 days. The resulting iPSC-derived chondrocyte organoids (iChOs) were fixed in 4% PFA, cryosectioned, and stained with H&E, Safranin O, Alcian Blue, and immunofluorescence.

2.4. RT-qPCR

Total RNA was extracted with TRIzol® (*Invitrogen*, USA), quantified by NanoDrop™ 2000 (Thermo Fisher Scientific), and reverse-transcribed using SPARKscript II RT Plus Kit (SparkJade, Qingdao, China). RT-qPCR was performed on QuantStudio™ 5 (Applied Biosystems, USA) with 2× SYBR® Green Premix (Accurate Biology, Changsha, China). GAPDH served as internal reference; relative expression was calculated by the $2^{-}\Delta\Delta Ct$ method. Primers are listed in Table 1.

2.5. Biochemical quantification, transcriptomic analysis, and experimental validation

Total sulfated GAG was quantified by DMMB assay (Haling Biotech, China); HS levels were measured using a human-specific ELISA kit (Cusabio, China). For transcriptomic profiling, total RNA was extracted from chondrocytes at day 21 of differentiation (three biological replicates per genotype) and sequenced on the Illumina NovaSeq 6000 platform (Novogene, China). Key differentially expressed genes identified by RNA-seq were validated at the mRNA level by RT-qPCR and at the protein level by Western blot analysis.

2.6. Statistical analysis

Data are mean ± SD from ≥ 3 biological replicates. Three-group comparisons used Kruskal–Wallis test

Table 1. Sequences of primers used in this study

Primers Target	Forward/Reverse primer (5′-3′)
OCT4	CCTCACTTCACTGCACTGTA/ CAGGTTTTCTTTCCCTAGCT
SOX2	CCCAGCAGACTTCACATGT/ CCTCCCATTTCCCTCGTTTT
NANOG	AAGGTCCCGGTCAAGAAACAG/ CTTCTGCGTCACACCATTGC
GAPDH	GTGGACCTGACCTGCCGTCT/ GGAGGAGTGGGTGTCGCTGT
P1/P2	GTGTCTCTTAAACTGTGCATC/ CTGAGTAGGTGTCATTCTAT
P3/P4	GCATACATTATACGAAGTTA/ ACAAATGTGGTATGGCTGAT
MIX-L1	GGATCCAGCTTTTATTTTCTCCCCT/ AGGAGCACAGTGGTTGAGGA
Brachyury	TATGAGCCTCGAATCCACATAGT/ CCTCGTTCTGATAAGCAGTCAC
Sox9	AAGATGACCGACGAGCAG/ CACGGGGAACTTGTCCT
ACAN	TGCAGAACAGTGCCATCA/ CTCCATAGCAGCCTTCCC
Col2a1	TCCCACCCTCTCACAGTTC/ TGCCCAGTTCAGGTCTCTT

with Dunn's post hoc correction; pairwise comparisons used Mann–Whitney *U* test (two-tailed). Analyses were performed in GraphPad Prism 9.0 (San Diego, CA, USA); $p < 0.05$ was significant.

3. Results and Discussion

3.1. Generation of an isogenic EXT1 biallelic mutant iPSC model

To investigate the phenotypic consequences of graded *EXT1* loss in a genetically controlled human system, we established an integrated CRISPR/Cas9–PiggyBac editing platform to introduce a second pathogenic mutation (c.1883+1G>T) into patient-derived iPSCs already carrying the heterozygous *EXT1* c.1126C>T mutation (Supplementary Figure S1, *https://www.biosciencetrends.com/action/getSupplementalData.php?ID=292*). Junction PCR with P1/P2 primers confirmed successful homologous recombination at the intended EXT1 locus in approximately 80% of screened clones. After hyPBase-mediated transposon excision, P3/P4 PCR showed no amplification, confirming complete removal of the selection marker. Sanger sequencing further verified the engineered c.1883+1G>T mutation (Figure 1A–D). The resulting iPSCs-DM retained expression of pluripotency markers (OCT4, NANOG, SSEA-4), normal karyotype, and tri-lineage differentiation potential (Supplementary Figure S2, *https://www.biosciencetrends.com/action/getSupplementalData.php?ID=292*), and differentiated efficiently into iMSCs and subsequently into chondrocytes (Supplementary Figure S3, *https://www.biosciencetrends.com/action/getSupplementalData.php?ID=292*).

Because WT, SM, and DM lines share an identical genetic background—differing exclusively at the engineered *EXT1* locus—all phenotypic differences are attributable solely to the introduced second hit. This isogenic single-variable design, achieved through footprint-free PiggyBac excision preserving endogenous genomic architecture, partially compensates for single-patient derivation and fundamentally distinguishes our approach from unmatched inter-individual specimen comparisons (*14–16*).

3.2. Biallelic EXT1 mutation disrupts HS biosynthesis and alters extracellular matrix content

To determine whether graded *EXT1* loss differentially affects HS biosynthesis and extracellular matrix (ECM) composition, we quantified HS and total GAG levels in day 21 chondrocyte cultures across all three genotypes. HS was markedly reduced in DM cell lysates and conditioned supernatants compared with WT ($p < 0.001$), with no significant difference between SM and WT (Figure 2A). This marked HS reduction in DM is consistent with the near-complete absence of HS immunostaining reported in human osteochondroma cartilage caps (*17*). Notably, total sulfated GAG as measured by the DMMB assay was markedly elevated in DM relative to WT and SM ($p < 0.0001$). Total sulfated GAG in cartilage comprises several species, predominantly chondroitin sulfate (CS) and keratan sulfate (KS), alongside the functionally critical heparan sulfate (HS). Because CS is the dominant GAG species on the major cartilage proteoglycan aggrecan, and HS was severely depleted in DM cells, the observed net increase in total sulfated GAG is most parsimoniously explained by a compensatory elevation of CS. Bachvarova *et al.* have clearly demonstrated this compensatory mechanism in *Ext1*-deficient mouse chondrocytes: $Ext1^{gt/gt}$ cells, which produce only approximately 20% of normal HS levels, exhibited a 70% increase in CS content and a 65% elevation in total GAG, accompanied by significant upregulation of aggrecan (*ACAN*) expression—aggrecan being the principal core protein carrying additional CS chains (*18*). Furthermore, Huegel *et al.* demonstrated that perturbation of HS function triggers cellular responses similar to *Ext* gene ablation, including enhanced chondrogenic differentiation and upregulation of cartilage-specific genes such as *ACAN* (*19*), consistent with the concurrent *ACAN* mRNA upregulation observed in our DM group.

3.3. EXT1 biallelic inactivation drives aberrant chondrogenesis in 2D and 3D culture systems

To investigate the functional consequences of *EXT1* loss on chondrocyte differentiation, we evaluated cartilage formation in both 2D monolayer and 3D organoid culture systems.

In 2D monolayer chondrogenic culture, WT and SM

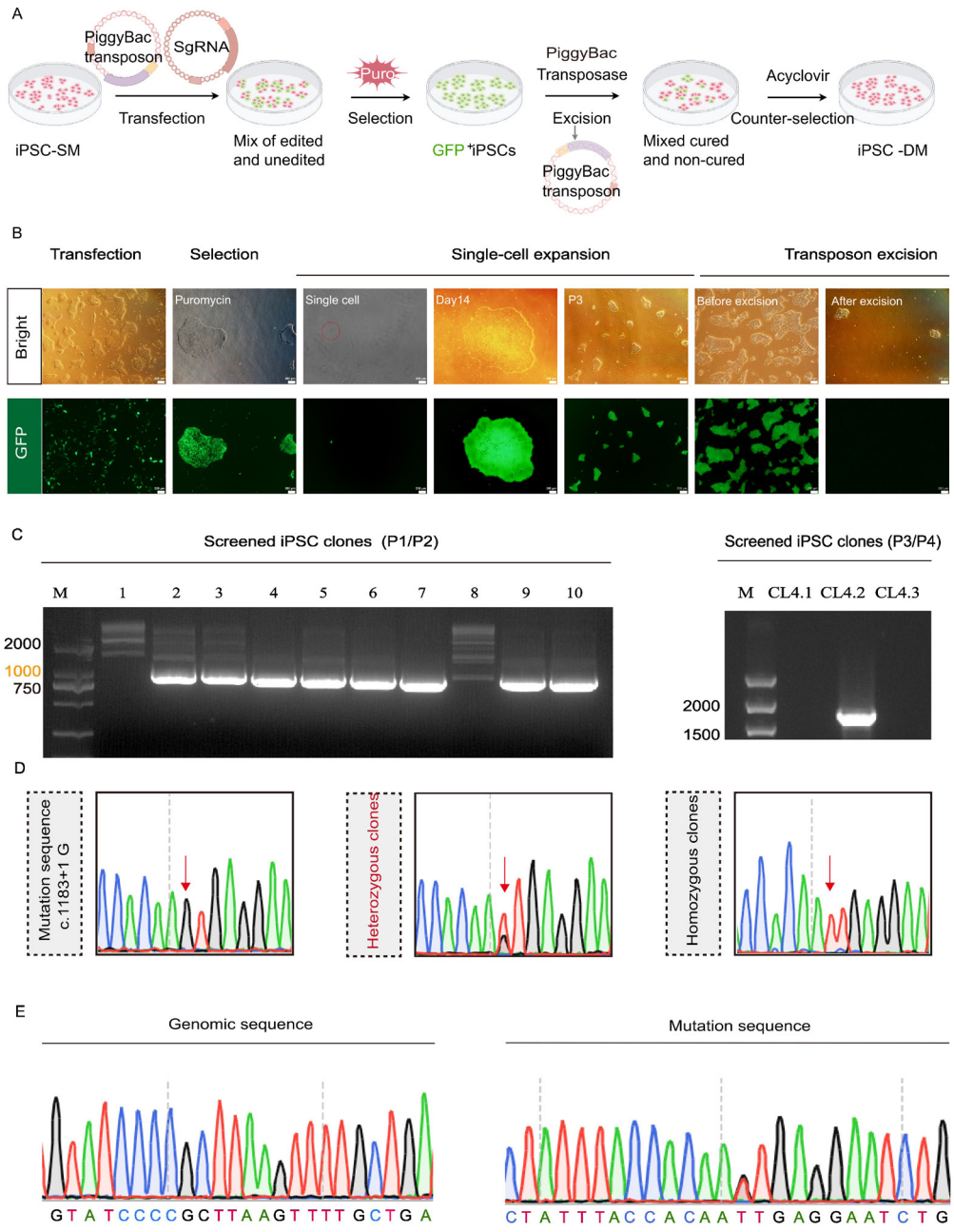

Figure 1. Genotypic validation of footprint-free EXT1 biallelic mutant iPSCs. (A) Schematic overview of the CRISPR/Cas9 and PiggyBac-mediated editing workflow. **(B)** Representative bright-field and fluorescence micrographs documenting GFP-positive integration and subsequent transposon excision. **(C)** PCR analysis confirming site-specific integration (P1/P2) and complete PiggyBac cassette excision (P3/P4). **(D)** Sanger sequencing chromatograms verifying the engineered c.1883+1G>T mutation in isolated clones. **(E)** Sanger sequencing confirming the footprint-free restoration of the native genomic sequence at the transposon integration site.

iMSCs underwent normal chondrogenic differentiation, whereas DM iMSCs exhibited markedly enhanced chondrogenic marker expression. Immunofluorescence analysis revealed significantly intensified ACAN signal and complete absence of EXT1 protein in iChOs-DM (Figure 2B). RT-qPCR demonstrated that *ACAN*, *SOX9*, and *COL2A1* mRNA levels were all significantly elevated in DM, most pronounced at day 21. *ACAN* and *SOX9* showed time-dependent progressive increases, while *COL2A1* was initially low at days 4 and 7 before sharp upregulation at day 21 (Figure 2C), suggesting that biallelic *EXT1* loss disrupts the normal temporal coordination of chondrogenic differentiation. Previous studies have reported consistent findings: *Ext1*-deficient periosteal progenitor cells displayed enhanced chondrogenic capacity (*16*), and simultaneous silencing of *EXT1* and *FGFR3* in ATDC5 cells similarly promoted chondrogenesis (*20*).

In 3D organoid culture, DM chondrogenic organoids (iChOs-DM) were visibly larger and exhibited irregular, asymmetric morphology compared with WT and SM organoids. H&E staining revealed marked internal structural disorganization in iChOs-DM. Safranin O and Alcian Blue staining demonstrated intense but spatially

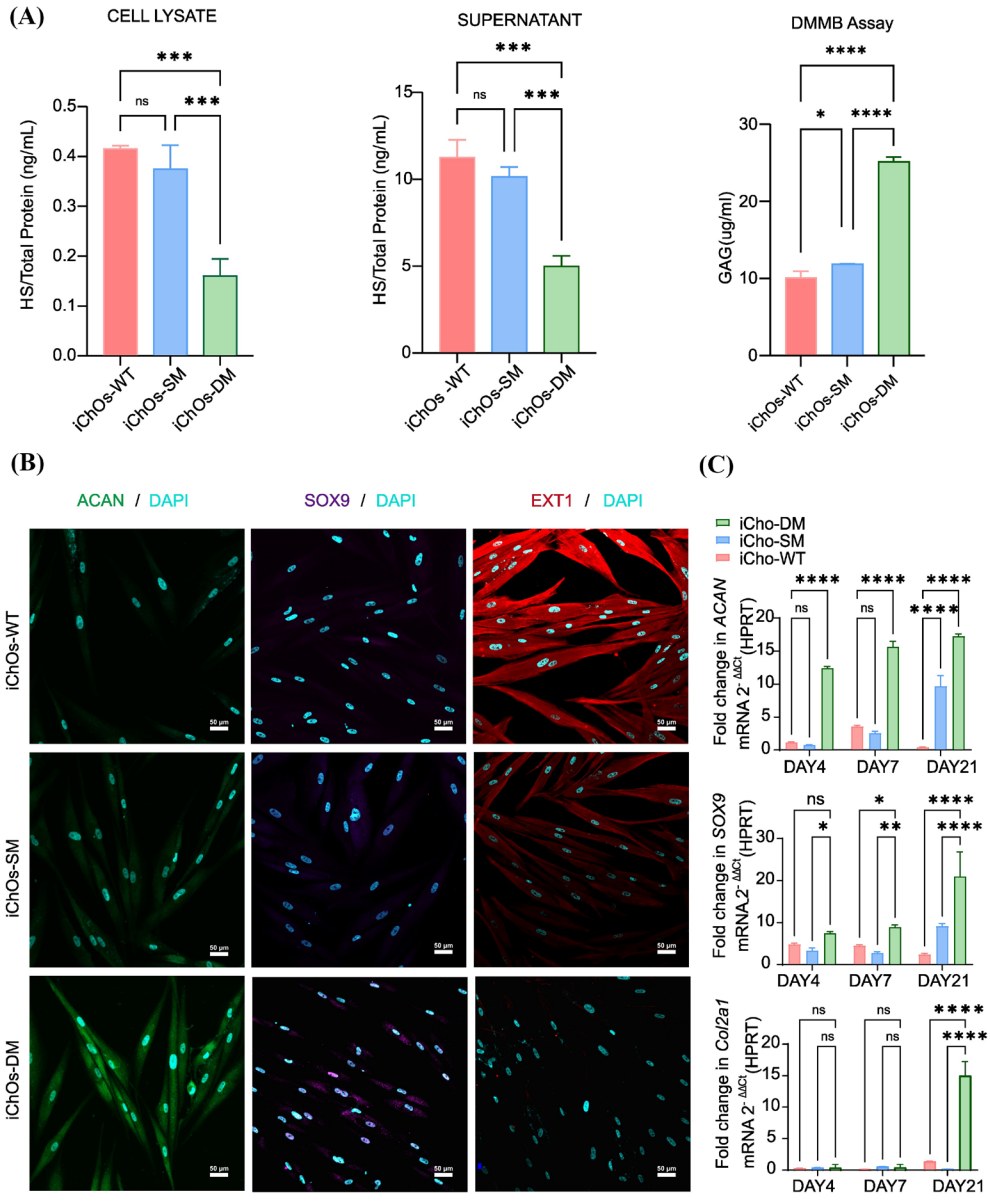

Figure 2. Biallelic *EXT1* inactivation disrupts ECM homeostasis and accelerates 2D chondrogenesis. (A) Quantification of HS by ELISA and total GAG by DMMB assay at day 21. **(B)** Immunofluorescence for ACAN (green), SOX9 (purple), and EXT1 (red) in 2D chondrocyte cultures. Scale bar: 50 µm. **(C)** RT-qPCR of *ACAN*, *SOX9*, and *COL2A1* at days 4, 7, 21. Data: mean ± SD; Kruskal–Wallis test with Dunn's post hoc correction.

heterogeneous proteoglycan deposition (Figure 3A), consistent with the approximately 50% GAG elevation reported in *Ext1*-hypomorphic mouse cartilage (*21*). Immunofluorescence confirmed markedly enhanced ACAN and complete EXT1 absence in iChOs-DM (Figure 3B). These phenotypic features partially recapitulate osteochondroma histopathology observed in *Ext1*-knockout mouse models (*14,22*).

Critically, SM iMSCs and organoids were indistinguishable from WT in both culture systems, and only DM exhibited accelerated chondrogenesis and tissue disorganization. This finding agrees with de Andrea *et al.* (*12*), who demonstrated that heterozygous *EXT* mutation does not impair chondrogenic differentiation and that osteochondroma formation is contingent upon LOH. Collectively, biallelic *EXT1* inactivation drives excessive chondrogenic gene expression, aberrant proteoglycan accumulation, and tissue architectural disruption, successfully recapitulating key pathological features of HMO *in vitro*.

3.4. Wnt signaling is the most significantly enriched pathway following EXT1 loss

To identify downstream signaling networks disrupted by *EXT1* loss, we performed transcriptomic profiling of day 21 chondrocytes. Comparative analysis identified substantial uniquely and overlappingly differentially expressed genes across genotypic transitions (Figure 4B), and principal component analysis (PCA) further

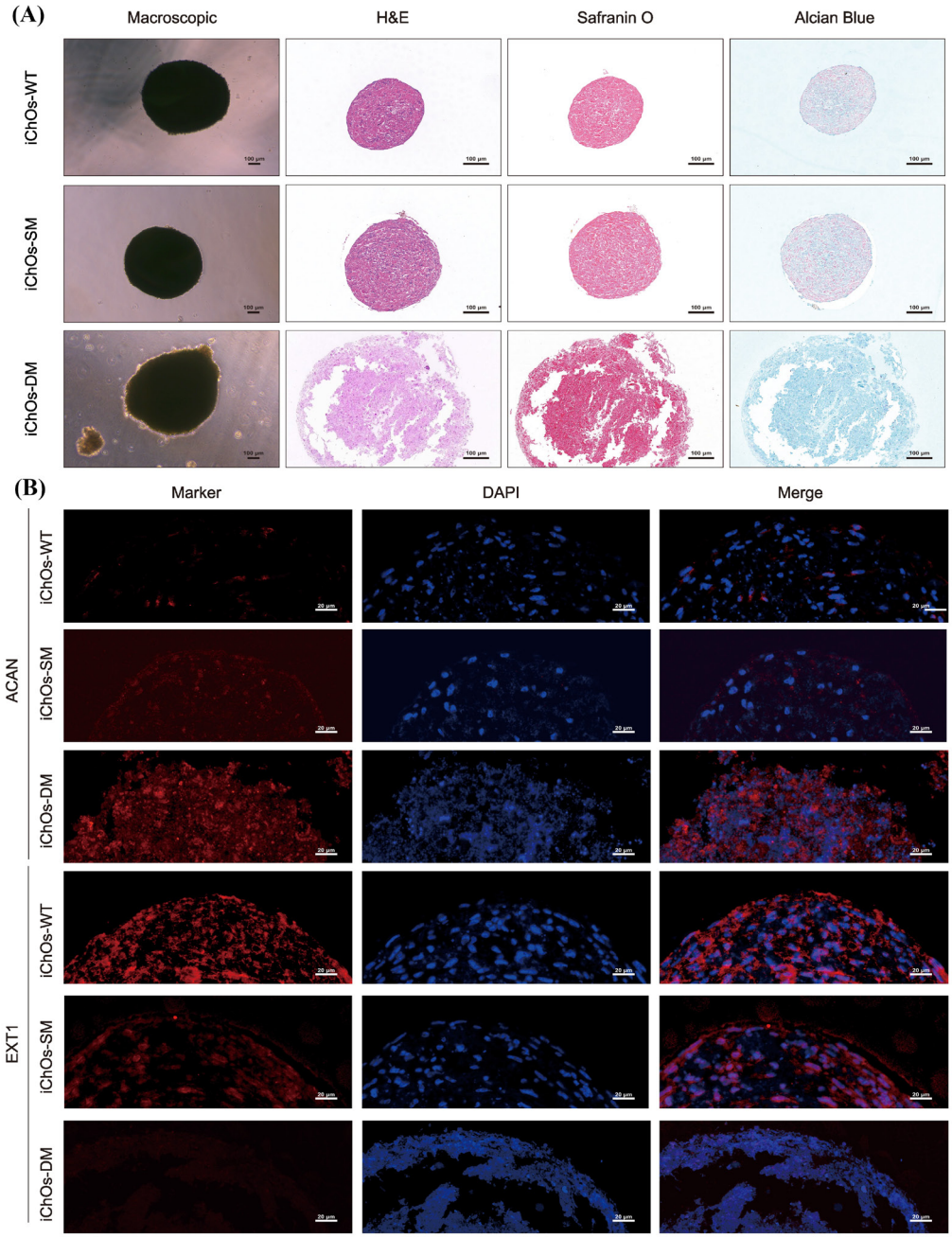

Figure 3. Complete *EXT1* loss promotes aberrant cartilage matrix deposition in 3D chondrogenic organoid culture. (A) Representative microscopic appearance of chondrogenic organoids at day 21 (top), H&E (second row), Safranin O (third row), and Alcian Blue (bottom row). Scale bar: 100 μm. **(B)** Immunofluorescence for ACAN (green) and EXT1 (red) with DAPI. Scale bar: 20 μm.

revealed distinct global expression signatures among the WT, SM, and DM groups (Figure 4C). We subsequently mapped the hierarchical clustering of core Wnt-related genes (Figure 4D), guided by KEGG pathway enrichment analysis which placed Wnt signaling as the most significantly enriched pathway (Figure 4E). Because HSPGs regulate Wnt ligand spatial distribution through differentially sulfated HS domains (*13,23*), these transcriptomic findings prompted targeted validation by RT-qPCR (Figure 4G).

Canonical Wnt ligands *WNT10B* and *WNT2B* were exclusively and significantly upregulated in DM ($p < 0.0001$), mirroring the DM-specific cartilage marker pattern (*24,25*). Secreted frizzled-related protein (*SFRP1* and *SFRP4*) mRNA levels were already markedly elevated in SM—higher than in DM—suggesting that partial HS reduction triggers compensatory Wnt antagonist upregulation. Despite elevated *SFRP4* mRNA in SM, SFRP4 protein was paradoxically lowest in SM (Figure 4F), likely reflecting active extracellular secretion for Wnt buffering (*26*). The β-catenin target *CCND2* (cyclin D2) was elevated at both mRNA and protein levels in DM (Figure 4F, G), confirming canonical Wnt/β-catenin activation (*27*). WNT10B protein did not

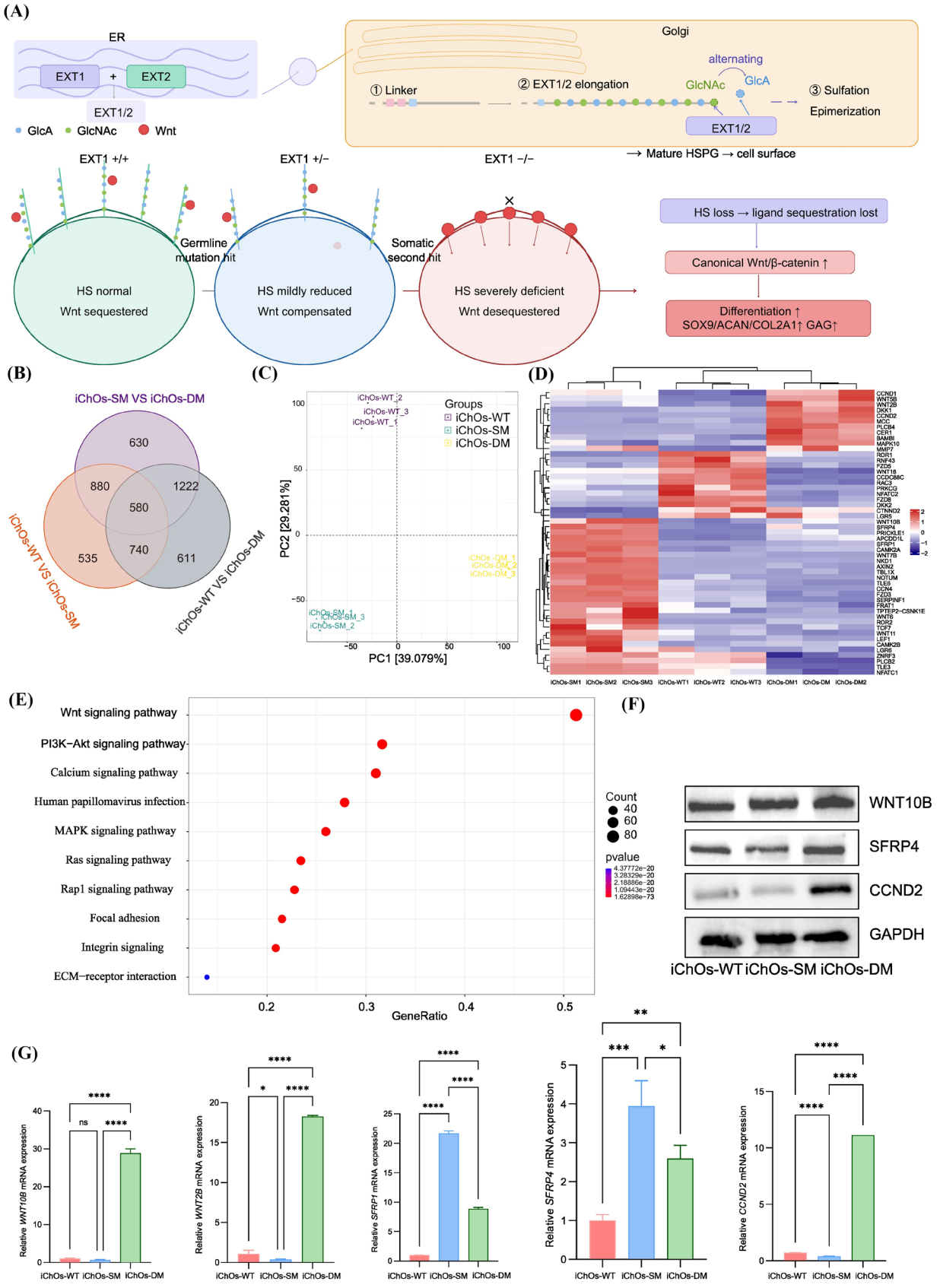

Figure 4. Transcriptomic analysis reveals Wnt signaling remodeling. (A) Schematic of the proposed EXT1/HSPG-dependent morphogen ligand sequestration model illustrating the consequences of graded EXT1 loss on canonical Wnt/β-catenin signaling (WT: intact gatekeeper; SM: compensated; DM: gatekeeper collapse). **(B)** Venn diagram. **(C)** PCA. **(D)** Heatmap. **(E)** KEGG enrichment. **(F)** Western blot: WNT10B, SFRP4, CCND2, GAPDH. **(G)** RT-qPCR: *WNT10B*, *WNT2B*, *SFRP1*, *SFRP4*, *CCND2*. Data: mean ± SD; Kruskal–Wallis with Dunn's correction.

proportionally mirror its mRNA, possibly due to loss of HSPG-mediated surface retention and accelerated extracellular release (*13,28*).

These data collectively support a "molecular gatekeeper" model in which HS sequesters morphogens—IHH, BMPs, FGFs, and Wnts—at the cell surface and within the pericellular matrix, maintaining signaling homeostasis (*7,13,28*). Approximately 50% of normal *EXT1* activity (SM) suffices to maintain this threshold; complete loss (DM) triggers a "signal eruption"—uncontrolled morphogen release overstimulating chondrogenesis (Figure 4A).

We propose a two-stage pathogenic framework. In the first stage ("priming"), germline heterozygous EXT1 mutation depletes the HS biosynthetic reserve without altering steady-state levels, thereby triggering compensatory SFRP1/4 upregulation—as evidenced by peak transcription in SM—sufficient to maintain normal differentiation. In the second stage ("triggering"), somatic second hit causes complete EXT1 inactivation and HS biosynthetic collapse. Compensatory SFRP buffering is overwhelmed: canonical Wnt ligands WNT10B and WNT2B are released in excess, and unrestrained canonical Wnt/β-catenin activation drives pathological chondrogenesis, concordant with LOH detection in 63% of clinical osteochondromas (*12*).

Mechanistically, HS loss simultaneously liberates canonical Wnt ligands and destabilizes SFRP antagonists whose stability depends on HSPG scaffolding (28). Gerstner *et al*. proposed an *EXT1*–Wnt regulatory feedback loop whose disruption may explain the explosive DM upregulation as overshoot compensation. The mRNA–protein discordance for WNT10B and SFRP4 can be explained by a unified mechanism: HS loss alters the extracellular fate of secreted canonical Wnt components—ligands lose surface tethering and undergo accelerated release, while antagonists exhibit reduced intracellular accumulation due to enhanced secretory flux. These findings further establish HS deficiency as a critical driver of canonical Wnt pathway dysregulation.

Notably, our use of iMSCs recapitulates periosteal mesenchymal progenitor differentiation, modeling the periosteal origin of osteochondromas (*14,16*)—a mechanism the traditional growth plate hypothesis cannot explain. Complete *EXT1* inactivation thus emerges as the decisive switch redirecting mesenchymal progenitor fate from osteogenic maintenance toward aberrant chondrogenesis.

In conclusion, by combining patient-derived iPSCs with footprint-free CRISPR/Cas9–PiggyBac editing, we demonstrate that complete EXT1 inactivation—not haploinsufficiency—is required to collapse HS-dependent morphogen gating, unleash canonical Wnt signaling, and drive pathological chondrogenesis. These findings provide direct human cellular evidence supporting the Two-hit model of HMO pathogenesis. However, as all iPSC lines derive from a single patient, validation across additional EXT1 or EXT2 genotypes is warranted. Furthermore, the *in vitro* system does not fully recapitulate the *in vivo* growth plate microenvironment; future studies employing *in vivo* transplantation and Wnt pathway modulation will be essential to evaluate therapeutic potential and model malignant progression toward secondary chondrosarcoma.

Acknowledgements

We sincerely thank Lingqun Ye, Ph.D., from Soochow University for kindly providing the original plasmids required for our gene editing research using the CRISPR-Cas9 and PiggyBac systems.

Funding: This work was supported by a grant from Shandong First Medical University (LJ001).

Conflict of Interest: The authors have no conflicts of interest to disclose.

References

1. Bovée JVMG. Multiple osteochondromas. Orphanet J Rare Dis. 2008; 3:3.
2. Schmale GA, Conrad EU, Raskind WH. The natural history of hereditary multiple exostoses. J Bone Joint Surg Am. 1994; 76:986-992.
3. Ahmed AR, Tan TS, Unni KK, Collins MS, Wenger DE, Sim FH. Secondary chondrosarcoma in osteochondroma: Report of 107 patients. Clin Orthop Relat Res. 2003; 411:193-206.
4. McCormick C, Duncan G, Goutsos KT, Bhatt L. The putative tumour suppressor EXT1 alters the expression of cell-surface heparan sulfate. Nat Genet. 1998; 19:158-161.
5. Lin X. Functions of heparan sulfate proteoglycans in cell signaling during development. Development. 2004; 131:6009-6021.
6. Bernfield M, Götte M, Park PW, Reizes O, Fitzgerald ML, Lincecum J, Zako M. Functions of cell surface heparan sulfate proteoglycans. Annu Rev Biochem. 1999; 68:729-777.
7. Koziel L, Kunath M, Kelly OG, Vortkamp A. Ext1-dependent heparan sulfate regulates the range of Ihh signaling during endochondral ossification. Dev Cell. 2004; 6:801-813.
8. Clement A, Wiweger M, von der Hardt S, Ruber MA, Crome A, Schulte-Merker S, Knust E. Regulation of zebrafish skeletogenesis by ext2/dackel and papst1/pinscher. PLoS Genet. 2008; 4:e1000136.
9. Knudson AG. Mutation and cancer: Statistical study of retinoblastoma. Proc Natl Acad Sci U S A. 1971; 68:820-823.
10. Zak BM, Schuksz M, Koyama E, Munoz C, De Jong DS, Koober DG, Pacifici M, Esko JD. Compound heterozygous loss of Ext1 and Ext2 is sufficient for formation of multiple exostoses in mouse ribs and long bones. Bone. 2011; 48:979-987.
11. Stickens D, Zak BM, Rougier N, Esko JD, Bhatt SR. Mice deficient in Ext2 lack heparan sulfate and develop exostoses. Development. 2005; 132:5055-5068.
12. de Andrea CE, Reijnders CMA, Kroon HM, de Jong

D, Hogéndoorn PCW, Szuhai K, Bovée JVMG. Secondary peripheral chondrosarcoma evolving from osteochondroma as a result of outgrowth of cells with functional EXT. Oncogene. 2012; 31:1095-1104.
13. Mii Y, Takada S. Heparan sulfate proteoglycans as Wnt co-receptors and their role in Wnt signaling. Front Cell Dev Biol. 2020; 8:631.
14. Jones KB, Piombo V, Searby C, Kurriger G, Yang B, Grabellus F, Roughley PJ, Morcuende JA, Buckwalter JA, Capecchi MR, Vortkamp A, Sheffield VC. A mouse model of osteochondromagenesis from clonal inactivation of Ext1 in chondrocytes. Proc Natl Acad Sci U S A. 2010; 107:2054-2059.
15. Matsumoto K, Irie F, Mackem S, Yamaguchi Y. A mouse model of chondrocyte-specific somatic mutation reveals a role for Ext1 loss of heterozygosity in multiple hereditary exostoses. Proc Natl Acad Sci U S A. 2010; 107:10932-10937.
16. Inubushi T, Nozawa S, Matsumoto K, Irie F, Yamaguchi Y. Aberrant perichondrial BMP signaling mediates multiple osteochondromagenesis in mice. JCI Insight. 2017; 2:e90049.
17. Huegel J, Sgariglia F, Enomoto-Iwamoto M, Koyama E, Dormans JP, Pacifici M. Heparan sulfate in skeletal development, growth, and pathology: the case of hereditary multiple exostoses. Dev Dyn. 2013; 242:1021-1032.
18. Bachvarova V, Dierker T, Esko JD, Hoffmann D, Kjellén L, Vortkamp A. Chondrocytes respond to an altered heparan sulfate composition with distinct changes of heparan sulfate structure and increased levels of chondroitin sulfate. Matrix Biol. 2020; 93:43-59.
19. Huegel J, Enomoto-Iwamoto M, Sgariglia F, Koyama E, Pacifici M. Heparanase stimulates chondrogenesis and is up-regulated in human ectopic cartilage: A mechanism possibly involved in hereditary multiple exostoses. Am J Pathol. 2015; 185:1676-1685.
20. Zhang F, Wang Y, Li T, Liu H, Chen W, Guo J. EXT1 and FGFR3 co-silencing promotes chondrogenesis in ATDC5 cells. Mol Med Rep. 2024; 29:7.
21. Gerstner M, Jouanno Y, Gericke M, Wienhold T, Dierker T, Osterhaus K, Gorsi HS. A cartilage-specific EXT1 mouse model recapitulates features of hereditary multiple osteochondromas. Bone. 2021; 143:115794.
22. Jones KB, Pacifici M, Hilton MJ. Multiple hereditary exostoses (MHE): Elucidating the pathogenesis of a rare skeletal disorder through interdisciplinary research. J Biomed Biotechnol. 2012; 2012:462049.
23. Mii Y, Nakazato K, Pack CG, Ikeda T, Makino Y, Ito A, Shimono C, Takada S. Asymmetric Wnt ligand distribution on the cell surface by heparan sulfate proteoglycans. eLife. 2022; 11:e73818.
24. Bennett CN, Ouyang H, Ma YL, Zeng Q, Gerin I, Sousa KM, Lane TF, Krishnan V, Hankenson KD, MacDougald OA. Wnt10b increases postnatal bone formation by enhancing osteoblast differentiation. J Bone Miner Res. 2007; 22:1924-1932.
25. Riedl M, Witzmann C, Koch M, Lang S, Kerschbaum M, Grifka J, Grässel S. WNT2B mediates chondrogenic commitment of human bone marrow-derived mesenchymal stromal cells. Sci Rep. 2020; 10:7113.
26. Nakanishi R, Shimizu M, Mori M, Akiyama H, Okudaira S, Otsuki B, Hashimoto M, Higuchi K, Watanabe M, Nishi H, Kondoh T, Sano S, Nakamura T. Secreted frizzled-related protein 4 is a negative regulator of peak BMD in SAMP6 mice. Sci Rep. 2016; 6:25198.
27. Day TF, Guo X, Garrett-Beal L, Yang Y. Wnt/beta-catenin signaling in mesenchymal progenitors controls osteoblast and chondrocyte differentiation during vertebrate skeletogenesis. Dev Cell. 2005; 8:739-750.
28. Üen A, Reichsman F, Anest V, Taylor WG, Muraiso K, Bottaro DP, Cumberledge S, Rubin JS. Secreted frizzled-related protein-1 binds directly to Wingless and is a biphasic modulator of Wnt signaling. J Biol Chem. 2000; 275:4374-4382.

Received February 10, 2026; Revised March 20, 2026; Accepted March 24, 2026.

Address correspondence to:
Jing Luan and Jinxiang Han, Biomedical Sciences College, Shandong First Medical University, Ji'nan, Shandong 250117, China.
E-mail: luanjing@sdfmu.edu.cn (JL); jxhan9888@aliyun.com (JH)

Yazhou Cui, Qingdao Academy of Chinese Medical Science, Shandong University of Traditional Chinese Medicine, Ji'nan, Shandong 250355, China; Biomedical Sciences College, Shandong First Medical University, Ji'nan, Shandong 250117, China.
E-mail: cuiyazhou@sdutcm.edu.cn

Released online in J-STAGE as advance publication March 26, 2026.